

# A Fast and Accurate Zebra Finch Syllable Detector

Ben Pearre<sup>1,a,✉</sup>, L. Nathan Perkins<sup>1,b</sup>, Jeffrey E. Markowitz<sup>2,c</sup>, Timothy J. Gardner<sup>1,d</sup>

<sup>1</sup> Department of Biology, Boston University, Boston, Massachusetts, United States of America

<sup>2</sup> Department of Neurobiology, Harvard Medical School, Boston, Massachusetts, United States of America

Author <sup>a</sup> contributed the original MATLAB and LabVIEW implementations and most of the manuscript. <sup>b</sup> contributed the Swift implementation and its description herein, helped debug the training code, and measured the timing for most of the detectors.

<sup>c</sup> performed the fibre photometry experiment, wrote several types of filter-bank software against which we compared, made suggestions for the neural network detector, and reformatted the MATLAB code for distribution. <sup>d</sup> provided a stream of suggested techniques, metrics, and goals.

✉ Corresponding author: bwpearre@gmail.com (BP)

## Abstract

The song of the adult male zebra finch is strikingly stereotyped. Efforts to understand motor output, pattern generation, and learning have taken advantage of this consistency by investigating the bird's ability to modify specific parts of song under external cues, and by examining timing relationships between neural activity and vocal output. Such experiments require that precise moments during song be identified in real time as the bird sings. Various syllable-detection methods exist, but many require special hardware, software, and know-how, and details on their implementation and performance are scarce. We present an accurate, versatile, and fast syllable detector that can control hardware at precisely timed moments during zebra finch song. Many moments during song can be isolated and detected with false negative and false positive rates well

under 0.5% and 0.01% respectively. The detector can run on a stock Mac Mini with triggering delay of less than a millisecond and a jitter of  $\sigma \approx 2$  milliseconds.

## 1 Introduction

The adult zebra finch (*Taeniopygia guttata*) sings a song made up of 2–6 syllables, with longer songs taking on the order of a second. The song may be repeated hundreds of times per day, is almost identical each time, and several brain areas reflect this consistency in highly stereotyped neural firing patterns. This consistency makes the zebra finch one of the most popular models for the study of the neural basis of learning, audition, and control.

This consistency allows a variety of experiments if precise moments in song can reliably be detected quickly enough to trigger other apparatus during singing. A common area of study with this song-triggering technique is the anterior forebrain pathway (AFP), a homologue of mammalian basal ganglia consisting of a few distinct brain areas concerned with the acquisition and learning of song. For example, [1] stimulated the lateral magnocellular nucleus of the anterior nidopallium (LMAN)—the output nucleus of the AFP—at precisely timed moments during song and showed that this area repeatably controls specific variables in song output. [2] stimulated LMAN and the high vocal centre (HVC) in one hemisphere or the other, and found that control of song rapidly switches between hemispheres. [3] investigated the response of cells in field L and the caudolateral mesopallium during song with and without feedback perturbations as well as external sounds, and concluded that these regions may hold a representation of song against which auditory signals are compared. [4] played a disruptive sound during renditions of a syllable that were slightly above (or below) its average pitch, and showed that the presence of this apparently random natural variability in songbird motor output is used to drive change in the song. [5] extended this experiment and showed that AFP produces a corrective signal to bias song away from those disruptions. [6] showed that that AFP transfers this signal to the robust nucleus of the arcopallium (RA) using NMDA-receptor-mediated glutamatergic transmission. By looking at song recovery after applying the same pitch-shift paradigm, [7] showed that the caudal medial nidopallium is implicated in

memorising or recalling a recent song target, but for neither auditory processing nor directed motor learning.

Despite the power and versatility of such experiments, there is no standard syllable detector. Considerations include:

**Accuracy:** How often does the system produce false positives or false negatives?

**Latency:** The average delay between the target syllable being sung and the detection.

**Jitter:** The amount that latency changes from instance to instance of song. Our measure of jitter is the standard deviation  $\sigma$  of latency.

**Versatility:** Is detection possible at “difficult” syllables?

**Ease of use:** How automated is the process of programming a detector?

**Cost:** What are the hardware and software requirements?

A variety of syllable-triggering systems have been used, but few have been documented or characterised in detail. In 1999, [8] used groups of IIR filters with hand-tuned logical operators. Their system had a latency of 50 or 100 milliseconds (ms), and they do not report on jitter or accuracy. As access to computational resources has improved, approaches have changed: in 2009, [5] still used hand-tuned filters, but ran them on a Tucker-Davis Technologies digital signal processor. They report a latency of around 4 ms, but as with other filter-bank techniques, it is not strictly a syllable detector but rather a pitch and timbre detector—it cannot identify a frequency sweep, or distinguish a short chirp from a long one—and thus requires careful selection of target syllables. Furthermore, the method is neither inexpensive nor, based on our experience with a similar technique, accurate. [3] applied a neural network to a spectral image of song. They report a jitter of 4.3 ms, but further implementation and performance details are not available. In 2011, [6] matched spectral templates to stable portions of syllables in 8-ms segments. They report a jitter of 4.5 ms, and false-negative and false-positive rates of up to 2% and 4%, respectively. Hardware requirements and ease of use were not reported. In 2013, [9] described in detail a system that matches spectral images of template syllables using a correlation coefficient. With a fast desktop (Intel i7 six-core) running Linux and

equipped with a National Instruments data acquisition card, it boasts a hardware-only (not accounting for the time taken to compute a match with a syllable) latency and jitter of just a few microseconds, and the detection computation they use should not much increase that. Drawbacks are that some hand-tuning may still be required, and that they report false-negative rates around 4% and 7% for zebra finches and Bengalese finches respectively, measured on a small dataset. In much other work, an allusion is made to a syllable detector, but no further information is provided.

We developed a standalone detector that learns to match moments in the song using a neural network applied to the song spectrogram, and outputs a TTL pulse (a brief 5-volt pulse) at the chosen moment. The approach consists of three steps:

1. Record and align a corpus of training songs. The technique has been published in [10].
2. Choose one or more instants in the song that should create a trigger event, and train a neural network to recognise them. This step is carried out offline. While any neural network software would produce equivalent results, we used MATLAB 2015b's neural network toolbox.
3. Once trained and saved, the neural network is used by a realtime detection program that listens to an audio signal and indicates detection of the target syllables via a TTL pulse. We present three implementations, in MATLAB, LabVIEW, and Swift, that trade off hardware requirements, ease of maintenance, and performance.

This method makes the following contributions:

- Fast: sub-millisecond latencies, with jitter around 2 ms.
- Accurate: false positive rates under 0.02% and false negative rates under 0.5% for a variety of syllables. Balancing these rates depends on a single relative-cost parameter.
- State-of-the-art performance with default parameters.
- Runs on inexpensive hardware.

- Described in detail here, with reference implementations provided and  
86  
benchmarked.  
87

## 2 Materials and Methods

  
88

### 2.1 Learning a detector

  
89

We begin with a few hundred recordings of a given bird's song, in this case made  
90  
inside a sound-isolating chamber in which was mounted a recording microphone  
91  
(Audio-Technica AT803). The songs are time-aligned as described in [10].  
92

We rely on two circular buffers:  
93

**Audio buffer:** This contains the most recent audio samples, and is of the length  
94  
required to compute the Fast Fourier Transform (FFT)—usually 256 samples.  
95

**FFT buffer:** The results of each new FFT are placed here. It contains the  $n_{\text{fft}}$  most  
96  
recent FFTs, which will serve as inputs to the neural network (described below).  
97

Audio is recorded at some sample rate  $1/t_{\text{sample}}$  (for example, 44.1 kHz), and new  
98  
data are appended to the circular audio buffer.  
99

The spectrogram is computed at regular intervals—the useful range seems to be  
100  
roughly 1–5 milliseconds, which we refer to as the frame interval  $t_{\text{fft}}$ . At each frame, a  
101  
spectrum is computed from the most recent 256 audio samples in the audio buffer, and  
102  
the result is appended to the FFT buffer. For example, if  $t_{\text{fft}} = 1$  ms and the recording  
103  
sample rate  $1/t_{\text{sample}} = 40$  kHz, then in order to compute a new FFT,  
104  
 $40000 \cdot 0.001 = 40$  new audio samples must be appended to the audio buffer, the FFT is  
105  
computed using the most recent 256 samples in that buffer, and the result is appended  
106  
to the FFT buffer. Over time, the successive spectra will look something like Fig. 1.  
107

Note that this results in time being discretised into chunks of length  $t_{\text{fft}}$ . Because  
108  
each Fourier transform computation contains a small number  $n_{\text{fft}}$  of new audio  
109  
samples (in the example above, 40 new samples and  $256 - 40$  that have already been  
110  
examined), we tried implementing the Sliding Discrete Fourier transform (SDFT) [11].  
111  
This allows  $t_{\text{fft}} = t_{\text{sample}}$ . Practically, the operating system retrieves new audio  
112  
samples from the hardware several at a time, so the full benefit of the SDFT is  
113  
difficult to see in practice. Furthermore, we found that FFT implementations are  
114

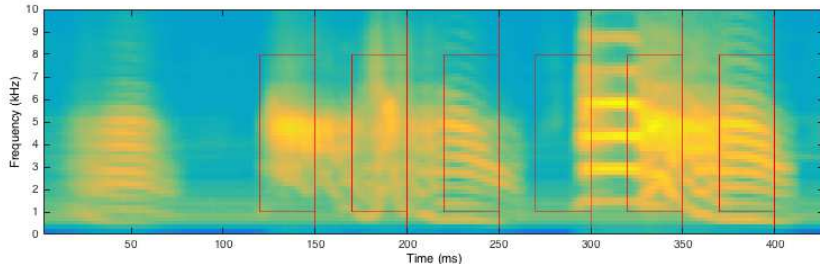


**Figure 1.** This image was made by superposing the spectra of our 2818 aligned songs. Our example detection points,  $t_1^* \dots t_6^*$ , are shown as red lines, with the recognition regions ( $30\text{ ms} \times 1\text{--}8\text{ kHz}$ ) marked as rectangles.

sufficiently highly optimised that discretising time into chunks of  $t_{\text{fft}}$  as we have done produced similar results with simpler software.

When using consumer audio hardware that operates best at 44.1 kHz, the requested frame interval may not line up with the sample rate, so the actual frame interval may be different from the intended. For example, at 44.1 kHz a 1-ms frame interval requires a new FFT every 44.1 samples. This must be rounded to 44 samples, resulting in  $t_{\text{fft}} = \lfloor 44.1 \rfloor / 44.1 \approx 0.9977$  ms.

One or more target moments during the song must be chosen. Our interface presents the time-aligned spectrogram averaged over training songs, and requires manual input of the target times,  $t^*$ . Then we assemble the training set from the song data, train the network, compute optimal output unit thresholds, and save the network object and an audio test file.

**Recognition region** The neural network's inputs are the FFT values from a rectangular region of the spectrogram covering a predefined range of frequency values  $F$  (for example, 1–8 kHz) at some number of the most recent frames  $n_{\text{fft}}$ . Any time  $t$  falls within frame  $\tau(t)$ , and  $t - t_{\text{fft}}$  falls within the previous frame, so the recognition region that the neural network receives as input consists of the spectrogram values over  $F$  at  $\tau(t)$  and those from the contiguous set of recent frames:  $T = \{\tau(t), \tau(t - t_{\text{fft}}), \tau(t - 2t_{\text{fft}}) \dots \tau(t - n_{\text{fft}}t_{\text{fft}})\}$ . We have found that a 30-ms time window—which will yield  $n_{\text{fft}} = |T| = \lfloor 30\text{ ms}/t_{\text{fft}} \rfloor$  frames—of frequencies spanning 1–8 kHz works well for most syllables.

Six examples of chosen target moments in the song, and their corresponding recognition regions  $F$  and  $T$ , are shown in Fig. 1.

**Building the training set** The training set is created in a fashion typical for neural networks: at each time frame  $t$  the rectangular  $|F| \times |T|$  recognition region in the spectrogram as of time  $t$  is reshaped into a vector  $\xi_t$ , which will have length  $|F||T|$  and contain the spectra in  $F$  taken at all of the times in the set  $T$ : from  $\tau(t - n_{\text{fft}}t_{\text{fft}})$  to  $\tau(t)$ . These vectors are placed into a training matrix,  $\Xi$ , such that each column  $\xi_t$  holds the contents of the recognition region—containing multiple frames from the spectrogram—as of one value of  $t$ .

Training targets  $y_t$  are vectors with one element for each desired detection syllable. That element is, roughly, 1 if the input vector comes from the target time ( $t = t^*$ ), 0 otherwise, for each target syllable (of which there may be any number, although they increase training time, and in our implementations the number of distinct output pulses is constrained by hardware). Since the song alignment may not be perfect, and due to sample aliasing, a strict binary target may ask the network to learn that, of two practically identical frames, one should be a match and the other not. Thus it is preferable to spread the target in time, such that at the target moment it is 1, and at neighbouring moments it is nonzero. We found that a Gaussian smoothing kernel around the target time with a standard deviation of 2 ms serves well.

With inputs well outside the space on which a neural network has been trained, its outputs will be essentially random. In order to reduce the false positive rate it is useful to provide negative training examples that include silence, cage noise, non-song vocalisations, and perhaps songs from other birds. Although it will depend on the makeup of the non-song data, we have found that training with as low as a 1:1 ratio of non-song to song yields excellent results.

**Normalisation** In order to present consistent and meaningful inputs to the neural network, we normalise the incoming data stream so that changes in the song structure of the sound are emphasised over changes in volume, and to maximise the effectiveness of the neural network’s training algorithm.

The first normalisation step is designed to eliminate differences in amplitude due to changes in the bird’s location and other variations in recording. Each recognition region vector  $\xi_t$ —during training, each *column* of the training matrix  $\Xi$ —is normalised using MATLAB’s `zscore` function  $\hat{\xi}_t = (\xi_t - \mu_{\xi_t})/\sigma_{\xi_t}$ , so that the content of each

window has mean  $\mu_{\hat{\xi}_t} = 0$  and standard deviation  $\sigma_{\hat{\xi}_t} = 1$ . 169

The second step is designed to ensure that the neural network's inputs have a 170 range and distribution for which the training function can easily converge. Each 171 element  $i$  of  $\hat{\xi}$  is normalised across the entire training set—each *row* of  $\Xi$ —in the same 172 way:  $\check{\xi}^i = (\hat{\xi}^i - \mu_{\hat{\xi}^i})/\sigma_{\hat{\xi}^i}$ , so that the values of that point across the whole training set 173 have mean  $\mu_{\check{\xi}^i} = 0$  and standard deviation  $\sigma_{\check{\xi}^i} = 1$ . This is accomplished during 174 training by setting MATLAB's neural network toolbox normalisation scheme to 175 `mapstd`, and the scaling transform is saved as part of the network object used by the 176 realtime detector so that it may be applied to unseen data at runtime. 177

These two normalisation steps provide a set of inputs that are more robust to 178 outliers and less likely to produce false positives during silence than other 179 normalisation schemes, such as linear or  $L_2$  normalisation. 180

**Neural Networks** While any learned classifier might suffice, we chose a two-layer feedforward neural network. In brief, our network takes an input vector  $\xi_t$ —as described above—and produces an output vector  $y_t$ , and when any element of  $y_t$  is above a threshold (described below), the detector reports a detection event. The network uses two matrices of weights,  $W_0$  and  $W_1$ , and two vectors of biases,  $b_0$  and  $b_1$ . The first takes the input  $\xi_t$  to an intermediate stage—the “hidden layer” vector. To each element of this vector is applied a nonlinear squashing function such as `tanh`, and then the second weight matrix  $W_1$  is applied. This produces output  $y_t$ :

$$y_t = W_1 \tanh(W_0 \xi_t + b_0) + b_1$$

During the network's training phase, the elements of the matrices and bias vectors are 181 learned by back-propagation of errors over a training set. A more detailed explanation 182 of neural networks may be found in [12]. 183

Essentially, after training, the network is available in the form of the two matrices 184  $W_0$  and  $W_1$  and the two vectors  $b_0$  and  $b_1$ , and running the network consists of two 185 matrix multiplications, two vector additions and the application of the squashing 186 function. 187

**Training the network** The network is trained using MATLAB's neural network toolbox. We tried a variety of feedforward neural network geometries, from simple 1-layer perceptrons to geometries with many hidden nodes, as well as autoencoders. Perhaps surprisingly, even the former yields excellent results on many syllables, but a 2-layer perceptron with a very small hidden layer—with a unit count 2-4 times the number of target syllables—was a good compromise between accuracy and training speed. For more variable songs, deep structure-preserving networks may be more appropriate, but they are slow to train and unnecessary for zebra finch song.

We used the Levenburg-Marquardt algorithm, which is the MATLAB toolbox's default. It is a fast algorithm, but is memory-intensive, so many target syllables or high FFT frame rates require a large amount of RAM and increase training time to hours. Other training algorithms that use less RAM are much slower, and by default they will often terminate prematurely due to their performance gradient going to 0.

**Computing optimal output thresholds** After the network is trained, outputs of the network for any input are now available, and will be in (or, due to noisy inputs and imperfect training, close to) the interval (0, 1). We must choose a threshold above which the output is considered a positive detection. Finding the optimal threshold requires two choices. The first is the relative cost of false negatives to false positives,  $C_n$ . The second is the acceptable time interval: if the true event occurs at time  $t$ , and the detector triggers at any time  $t \pm \Delta t$ , then it is considered a correct detection. Then the optimal detection threshold is the number that minimises [false positives] +  $C_n \cdot$  [false negatives] over the training set, using the definitions of false positives and negatives given in Section 2.3. Since large portions of the cost function are flat, hillclimbing is ineffective. Random-restart hillclimbing would work, but a brute-force search requires fractions of a second. For the results presented here, we have used  $C_n = 1$  and  $\Delta t = 10$  ms.

**De-bouncing** During runtime, the network may produce above-threshold responses to nearby frames. Thus, after the first response, subsequent responses are suppressed for 100 ms. However, for the accuracy figures presented here, we used the un-de-bounced network response.

**Our parameter choices** We used an FFT of size 256; a Hamming window; and  
218 chose a target spectrogram frame interval of  $t_{\text{fft}} = 1.5$  milliseconds, resulting in a true  
219 frame interval of  $t_{\text{fft}} = [1.5 \cdot 44.1]/44.1 \approx 1.4966$  ms. We set the network's input space  
220 to 30 ms long, and to span frequencies from 1–8 kHz, which contains the fundamentals  
221 and several overtones of most zebra finch vocalisations.  
222

We found these parameters to work well across a variety of target syllables, but  
223 various other parameter sets yield results similar to those presented here. Some of the  
224 parameters trade off detection accuracy or temporal precision vs. training time. For  
225 example, decreasing the frame interval generally decreases both latency and jitter, but  
226 also increases training time.  
227

## 2.2 Realtime detection

  
228

The architecture of the realtime detector requires that the most recent  $n_{\text{fft}}$   
229 spectrograms be fed to the neural network every frame interval. Audio samples from  
230 the microphone are appended to the circular audio buffer. Every  $t_{\text{fft}}$  seconds a new  
231 spectrogram is calculated by applying the Hamming window to the contents of the  
232 buffer, performing an FFT, and extracting the power. Outputs of the spectrogram  
233 from the target frequency band are appended to the circular FFT buffer. The  
234 spectrograms are sent to a static implementation of the previously trained neural  
235 network.  
236

We tested three implementations of the realtime detector. For all of these tests, we  
237 ran the detector processes under the operating systems' default schedulers and process  
238 priorities, running typical operating system daemon processes but no user loads. The  
239 computers had ample memory resources.  
240

**Swift** This detector uses the Swift programming language and Core Audio interface  
241 included in Apple's operating systems.  
242

The Core Audio frameworks provide an adjustable hardware buffer size for reading  
243 from and writing to audio hardware (different from our two circular buffers). Tuning  
244 this buffer size provides a tradeoff between the jitter in the detection and the  
245 processor usage needed to run the detector. We used buffer sizes ranging from 8  
246 samples (0.18 ms at 44.1 kHz) to 32 samples (0.7 ms at 44.1 kHz) depending on the  
247

frame size used by the detector.

Vector operations—applying the Hamming window, the FFT, input normalisation, matrix multiplication, and the neural network’s transfer functions—are performed using the Accelerate framework (vDSP and vecLib), which use modern vector-oriented processor instructions to perform calculations.

When the neural network detects a match, it instructs the computer to generate a TTL pulse that can be used to trigger downstream hardware. This pulse can be either written to the computer’s audio output buffer (again, in 8- to 32-sample chunks) or sent to a microcontroller (Arduino) via a USB serial interface. Sending the trigger pulse via the serial interface and microcontroller is noticeably faster (2.2 ms lower latency), likely due to the fact that the audio buffer goes through hardware mixing and filtering prior to output.

The above code can be run on multiple channels of audio on consumer hardware (such as a 2014 Mac Mini) with little impact on CPU usage (< 15%). Depending on the experimental needs, latency can potentially be further decreased (at the expense of processor usage) by adjusting the audio buffer sizes.

We ran the Swift detector on a Late 2014 Mac Mini with a Intel Core i5 processor at 2.6GHz with 16 gigabytes of RAM, running Mac OS X 10.11.

**LabVIEW** This implementation requires special software and hardware: LabVIEW from National Instruments—we used 2014 service pack 1—and a data acquisition card—we use the National Instruments PCI-6251 card on a PC with an Intel Core i5-4590 processor at 3.7GHz (a relatively low-end machine) with 32 gigabytes of RAM, running Microsoft Windows 8.1 Pro.

This implementation has several drawbacks: it requires Windows and expensive hardware and software and due to the programming language it is difficult to modify and debug—indeed, a persistent bug in our implementation currently renders it substantially less accurate than the other detector implementations on some syllables. However, our test configuration usually achieved excellent performance, and further gains should be possible if the implementation were retargeted onto field-programmable gate array (FPGA) hardware—which would have the additional benefit of providing deterministic “hard realtime” guarantees—or just run on a faster

desktop system.

279

**MATLAB** This detector uses the built-in audio input and output hardware on a compatible computer. We tested on a 2014 Mac Mini (the same machine used for the Swift detector described above) and 2015 Mac Pro. The Mac Pro does not have an audio input jack, so input was through an M-Audio MobilePre external USB audio interface. Despite the faster processor, the latter system did not achieve higher performance than the former, due to USB data transfer overhead.

280  
281  
282  
283  
284  
285

Because of how MATLAB's DSP toolbox interfaces with audio hardware, there is a double buffer both reading from and writing to audio hardware. As a result, much of the code focuses on a lightweight audio hardware interface, in order to have the smallest achievable audio buffer. To help achieve this, the MATLAB implementation spreads data acquisition and processing across two threads, due to the higher computational overhead of the interpreted programming language.

286  
287  
288  
289  
290  
291

The most versatile implementation, MATLAB runs on a variety of hardware and operating systems, and is perhaps the easiest to modify. While it did not perform as well on our test system as the other implementations, the convenience may outweigh the slight timing performance penalty for some experiments. Key to minimising jitter is the size of the audio buffer: on a 2014 Mac Mini running MATLAB 2015b the smallest buffer size that did not result in read overruns was about 4 ms.

292  
293  
294  
295  
296  
297

Similar to the Swift implementation, it is also possible to modify the MATLAB implementation to generate the TTL pulse from a microcontroller (Arduino) controlled via a serial over USB interface. This eliminates the double buffer required when sending triggers via the audio interface, reducing latency by half.

298  
299  
300  
301

### 2.3 Quantification

302

We divided the data into training and test sets. For the results reported in the following section, the training set consisted of 1000 instances of the song of one bird. Our test set consisted of an additional 1818 iterations of the bird's song.

303  
304  
305

The MATLAB neural network toolbox further divides our “training” set into internal training, validation, and test sets. We did not stray from the toolbox's default values, and do not discuss MATLAB's internal subdivision of our training set.

306  
307  
308

Because the dataset consists of temporally aligned songs, ground truth is available for  
309 each song (albeit with minor variations due to the alignment process used [10]), and  
310 thus the detector can be checked by presenting the recorded training songs as well as  
311 the canonical detection events. To this end, besides the trained network object, our  
312 learning code produces an audio file consisting of all of the training data on the left  
313 audio channel and a delta function at each aligned moment of target syllable  
314 presentation on the right channel. Thus, when played on any audio player, the left  
315 channel may be provided as input to the detector, and the the detector's output pulses  
316 may be compared against the right channel.  
317

**Accuracy** We define the accuracy of the network based on its classification  
318 performance per frame. In order to avoid the apparent problem of every non-detected  
319 non-syllable counting as a true negative, we also tried defining accuracy on a per-song  
320 basis, such that a song without the target syllable counted as a single true negative.  
321 Computing the optimal output thresholds on a per-frame basis resulted in higher  
322 thresholds and thus a lower false-positive rate, with minimal consequences to the  
323 false-negative rate, while also providing a valid definition of false-positive rate for data  
324 streams that had not been segmented into songs.  
325

The accuracy as defined above is used for computing the optimal thresholds above  
326 which the network's output should be interpreted as a match on the training data as  
327 described in Section 2.1, for evaluation of the detectors on the training songs, and  
328 while live.  
329

**Timing** We evaluate the time taken from the presentation of the target syllable to  
330 the firing of the detector's TTL pulse. While playing the audio test file from any  
331 audio playback device, the TTL output from the ground-truth channel of the audio  
332 output may be used as the trigger pulse for an oscilloscope, and compared to the TTL  
333 pulse produced by the detector implementation, which sees only the birdsong channel  
334 of the audio file. For this purpose we used a pulse generator (Philips PM 5715, with a  
335 listed latency of 50 ns, jitter of  $\leq 0.1\%$  or 50 ps, whichever is greater) to widen the  
336 detector's output spike to a number much larger than the jitter ( $\sim 100$  ms). This  
337 obviates pulse length variability in the output device by essentially discarding the  
338

falling edge of the output pulse. The oscilloscope is then set to averaging mode  
339  
(128-trigger average) in order to collect timing data. The canonical signal is the trigger  
340  
at  $t = 0$ , and the average of the detector's detection events will be seen as a  
341  
low-to-high transition with form approximating the cumulative probability  
342  
distribution function (CDF) of the detector's output in response to the chosen song  
343  
event, with individual detection events visible as steps in this curve.  
344

Mean latency is then given as the average time between the canonical signal and  
345  
the corresponding detection event. It is a helpful number, but not a critical one, since  
346  
a detector with high but constant latency can often be trained to trigger at a point  
347  
somewhat before the true moment of interest, especially given the stereotypy of zebra  
348  
finch song. Often more important is latency jitter: how much variability is there in the  
349  
latency? We define jitter as the standard deviation of the latency.  
350

When measuring timing, it is useful to compare against a theoretical optimal, in  
351  
order to control for any imprecision in the song extraction and alignment of our real  
352  
data inherent in the method we use (described in [10]). We propose two measures  
353  
thereof:  
354

First we test the “ideal” latency and jitter in the time shift used in calculating new  
355  
columns of the spectrogram. By passing a recorded audio sequence into the detector  
356  
offline, and assuming no input or output latency, we compare how many additional  
357  
audio samples beyond the syllable are needed before the spectrogram can match the  
358  
inputs needed to trigger the neural network. This latency reflects the FFT size used  
359  
for calculating the spectrogram, the FFT time shift between columns in the  
360  
spectrogram, and the width of the Gaussian smoothing kernel applied to the ground  
361  
truth data when training the neural network, but ignores computation times, audio  
362  
buffers, and other operating system overhead.  
363

Next we use a “ $\delta$ -syllable” consisting of a  $\delta$  function in the time domain, and train  
364  
the network to trigger 5 ms after this pulse. This song is fed into the live detector.  
365  
The results for this measurement show the latency and jitter inherent in the complete  
366  
detector including audio read and write buffers, classifier computation, and FFT time  
367  
shift aliasing, but excluding imprecision in the song alignment as well as detection  
368  
timing effects due to differences between instances of the bird's song.  
369

Finally, we measure latency on real bird song aligned as in [10]. This extracts and  
370

aligns the centres of the sampled songs, and the canonical signal is given with respect  
371  
to that alignment. These timing measurements reflect not only detector performance,  
372  
but also the variability of the bird's song.  
373

## 2.4 Fibre Photometry

In addition to synthetic tests of detector accuracy and latency, we piloted the syllable  
374  
detector in an experiment providing altered auditory feedback (AAF) to zebra finches.  
375  
AAF, or playback of a perturbing white noise stimulus, is known to disrupt the  
377  
highly-stereotyped zebra finch song. By probabilistically targeting the AAF to a  
378  
specific syllable, it is possible to selectively destabilize parts of the song. During this  
379  
feedback, signal from genetically-encoded calcium indicators was recorded via fibre  
380  
photometry to identify a neural representation of an error signals associated with the  
381  
feedback.  
382

The initial experiment design used a DSP with hand-designed filter-banks to detect  
383  
syllables, but these required tuning and were only conducive to detecting harmonic  
384  
stacks. This experiment provided an ideal design to pilot our neural-network-based  
385  
syllable detector.  
386

**Surgery** GCaMP6s and GCaMP6f were expressed using a lentivirus under the RSV  
387  
promoter [13]. Injections were targeted under HVC using stimulation of Area X with a  
388  
bipolar stimulation electrode. After injecting the virus, we implanted a fibre-optic  
389  
cannula above HVC (400 $\mu$ m diameter, Doric Lenses). The location of the injection  
390  
was verified histologically after each experiment.  
391

**Photometry** Fibre photometry [14–18] was performed in N=3 birds at least 2 weeks  
392  
post-injection using a completely fibre-coupled light path. A 470 nm fibre-coupled  
393  
LED (Mightex) was sinusoidally driven at 5 kHz by a TDT RX8. The output of the  
394  
LED was filtered with a GFP excitation filter (Doric Lenses Fluorescence Cube) and  
395  
coupled to an optical rotary joint (Doric Lenses). The rotary joint was connected via a  
396  
multimode fibre optic patch cord (400  $\mu$ m, .48 NA, Doric Lenses) to the implanted  
397  
cannula using a brass sleeve (Doric Lenses). LED power was calibrated such that  
398  
optical power at the tip was 20–300  $\mu$ W (LED was turned on only during  
399

vocalizations, detected using a TDT RX8). Fluorescence was collected through the  
400 same patch cord, filtered with a GFP emission filter, and sent to a silicon  
401 photomultiplier (SensL MiniSM 30000). The output of the photomultiplier was  
402 demodulated using a dual-phase lock-in amplifier (10-ms time-scale, SR830, Stanford  
403 Research Systems) and digitized along with the bird's song at 24.414 kHz using a  
404 National Instruments data acquisition board (PCIE-6323).  
405

**Syllable detection** User-selected syllables were detected using the Swift  
406 implementation of the syllable detector, and the TTL output triggered altered  
407 auditory feedback via the TDT RX8.  
408

**Data analysis**  $\Delta F/F_0$  was estimated at each point by subtracting and dividing by  
409  $F_0$ , defined as the 11th percentile computed in a 300-ms sliding window. Data were  
410 then smoothed with a 50-ms exponential window. Fluorescence traces during singing  
411 were normalized by subtracting the trial-average signal, in order to remove song-based  
412 modulation.  
413

## 2.5 Ethics

All procedures were approved by the Institutional Animal Care and Use Committee of  
415 Boston University (protocol number 14-029).  
416

## 3 Results

Fig. 1 shows the song for which we present accuracy and timing results. Six example  
418 target trigger points are shown, at 150, 200, 250, 300, 350, and 400 milliseconds after  
419 the beginning of the aligned samples, as indicated by the red lines, and referred to  
420 henceforth as  $t_1^* \dots t_6^*$  respectively. The rectangles show the recognition window (30  
421 ms, 1–8 kHz) for each instant in the song.  
422

The first two triggers,  $t_1^*$  at 150 ms and  $t_2^*$  at 200 ms, are far from pure tones, but  
423 are closer to coloured noise. They would be difficult for a harmonic-stack filter bank  
424 to detect, and especially to pinpoint in time.  $t_3^*$  (250 ms) and  $t_6^*$  (400 ms) are rich in  
425 overtones and contain downward slides with changing timbres.  $t_4^*$  (300 ms) occurs near  
426

the beginning of a more typical harmonic stack amenable to a variety of recognition  
427  
techniques, although consistently detecting a point partway through the syllable  
428  
demands a detector that can use multiple time steps.  $t_5^*$  (350 ms) shows a steady pitch  
429  
followed by a complex changing tone structure.  
430

An example of the detector's output for three of these syllables is shown in Fig. 2.  
431  
The total audio energy of each song is shown as a single grayscale row. By sorting  
432  
according to time of each syllable's detection, the rest of the song is shown in the  
433  
context of the timing for that moment. This gives an intuition of the timing variability  
434  
within each song and across songs (which may be responsible for some of our measured  
435  
jitter).  
436

### 3.1 Accuracy

We allowed our training software to allocate our default of 4 hidden units per syllable,  
438  
and computed a new FFT every 1.5 ms. Because our timing test files are designed for  
439  
our stereo playback software, allowing only one channel for the ground-truth pulse, we  
440  
trained one detector for each syllable for the following results. In order to eliminate  
441  
the large number of variables involved in microphone, cage, playback and re-digitising,  
442  
we evaluated the neural network's accuracy directly on the digitised recording. When  
443  
training and runtime data are gathered on the same hardware setup, this is the digital  
444  
signal that the detector will see—only the non-song data may be different.  
445

Accuracies for our six test syllables are shown in Fig. 3 (accuracies for the  
446  
synthetic  $\delta$ -function songs were always 100%). For each test syllable we trained 100  
447  
different networks, which differ from each other in the random initialisation of network  
448  
weights and on which random subset of our songs was used for training. Each  
449  
network's accuracy is shown as a single point in each chart in Fig. 3. Some syllables  
450  
are easier to identify reliably than others, allowing detection point choice to impact  
451  
the detector's accuracy. For difficult syllables, the training process occasionally yields  
452  
a network that performs unusually poorly, but it is easy to spot these networks by  
453  
their performance either as measured as part of the training process or on the test  
454  
audio file, and re-train when necessary.  
455

We repeated the above experiment using only 2 hidden units per syllable. Training  
456

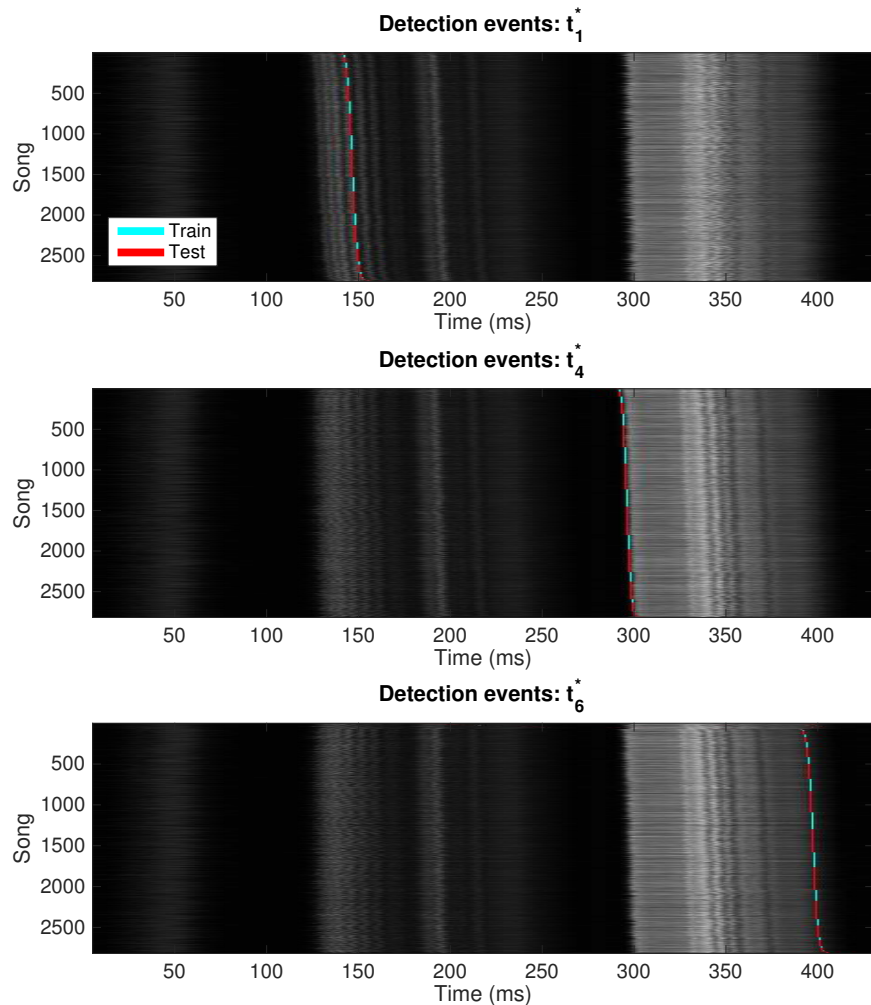


**Figure 2.** Each plot shows one network output unit's responses to all 2818 presentations of the song shown in Fig. 1. For simplicity, we show only the syllables  $t_1^*$ ,  $t_4^*$ , and  $t_6^*$ . The horizontal axis is time relative to the beginning of the aligned song, and the vertical axis is an index for the 2818 individual song presentations. The grey shading shows the audio amplitude of song Y at time T. Detection events on training songs are shown in cyan, with detections of unseen test songs in red. To provide an intuition of intra-song variability, songs have been stably sorted by the time of detection events; thus, each of the three detection graphs shows the songs in a different order.

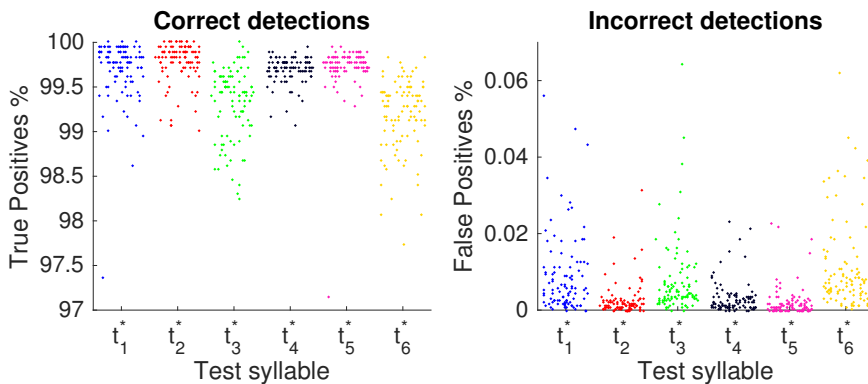


**Figure 3.** Accuracy variability over 100 different training runs for each of the six test syllables. Each dot shows the test-set accuracy for an independently trained detector. Because the horizontal positions have been randomised slightly so as not to occlude same-valued measurements, test syllable is also indicated by colour.

under this condition is much faster, but the mean true positive rate per syllable  
decreases by an average of 18% across our test syllables, and the mean false positive  
rate increases by roughly 23%.  
457  
458  
459

### 3.2 Timing

We evaluate variability in timing performance across three variables: FFT frame  
interval; syllable choice; and detector implementation.  
460  
461  
462

**FFT frame interval** Detector latency and jitter depend on the FFT frame rate.  
Our 1.5-ms-frame default is a compromise: shorter frames increase the precision of  
timing, but also increase computational requirements both during training and at  
runtime. Fig. 4 shows how these numbers vary over a useful range of frame rates on  
our ideal detector, the Swift detector with serial output, and for the LabVIEW  
detector, for both the  $\delta$ -syllable and for the bird song at  $t_4^*$ .  
463  
464  
465  
466  
467  
468

**Syllable choice** Syllable choice impacts detector performance, but despite the  
variety of syllables chosen here, performance was fairly stable across syllables. Fig. 5  
shows measured timing data for the Swift+serial detector compared to the ideal, with  
 $t_{\text{fft}} = 1.5$  ms. Given the variety of the test syllables, the variability is surprisingly low,  
and is summarised here with 95% confidence intervals (with  $n=6$ ):  
469  
470  
471  
472  
473

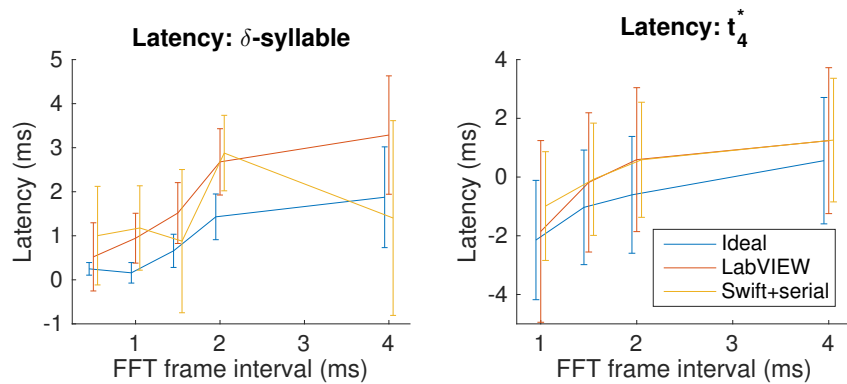


**Figure 4.** Timing varies as the FFT frame interval changes. Here we show results for the ideal detector and the LabVIEW and Swift+serial implementations, for the constructed  $\delta$ -syllable and for trigger  $t_4^*$  of the bird song. The lines show latency; error bars are standard deviation (jitter). Points have been shifted horizontally slightly for clarity; original positions are [0.5 1 1.5 2 4] ms.

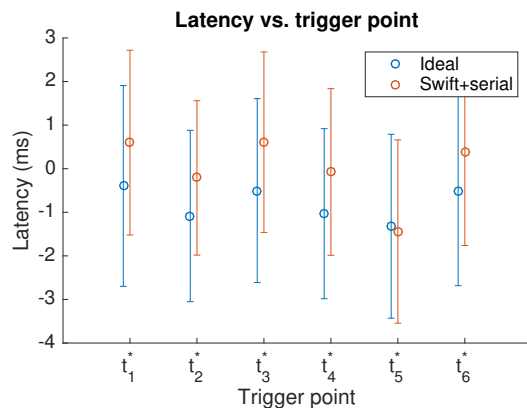


**Figure 5.** Timing data for our 6 test syllables, for the ideal and the Swift+serial detectors, with an FFT frame rate of 1.5 ms. Point centres show latency; error bars show jitter.

Detector	Latency	Jitter
Ideal	$-0.8 \pm 0.3$ ms	$2.1 \pm 0.1$ ms
Swift+serial	$0.0 \pm 0.6$ ms	$2.0 \pm 0.1$ ms

The negative latency is due to the way in which the network responds to the song through time: as the recognition region looks increasingly similar to the trained match, the network's evaluation of similarity rises, and will generally cross the triggering threshold before it reaches its maximum value. A heuristic as simple as triggering at an apparent turning point after crossing the threshold might improve timing consistency at the expense of latency, but we did not test this.

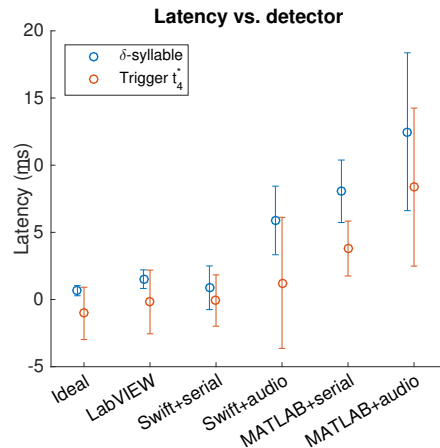


**Figure 6.** The different detectors for the constructed  $\delta$ -syllable and for the bird song at  $t_4^*$ . Point centres show latency; error bars show jitter.

**Detector Implementations** We compared latency and jitter across our different detector implementations for the  $\delta$ -syllable and  $t_4^*$ , again with  $t_{\text{fft}} = 1.5$  ms. Results are as follows:

Detector	$\delta$ -syllable		Bird: $t_4^*$	
	Latency (ms)	Jitter (ms)	Latency (ms)	Jitter (ms)
Ideal	0.66	0.38	-1.0	2.0
LabVIEW	1.5	0.69	-0.18	2.4
Swift+serial	0.88	1.6	-0.075	2.0
Swift+audio	5.9	2.6	1.2	4.9
MATLAB+serial	8.1	2.3	3.8	2.0
MATLAB+audio	13	5.9	8.4	5.9

These data are also plotted in Fig. 6, and Fig. 7 gives a more detailed view of what the timing curves look like for the five implementations of our detector on  $t_4^*$ .

### 3.3 Fibre Photometry

Fig. 8 shows 1,123 song performances from a single bird. At trial 858, the altered auditory feedback (AAF) was introduced, triggered by the first syllable in the song. Measurements of the fluorescence from genetically encoded calcium indicators in the HVC shelf reveal an AAF-sensitive response as compared with catch trials (Fig. 9). This suggests a population of cells in the HVC shelf that respond to AAF and may be

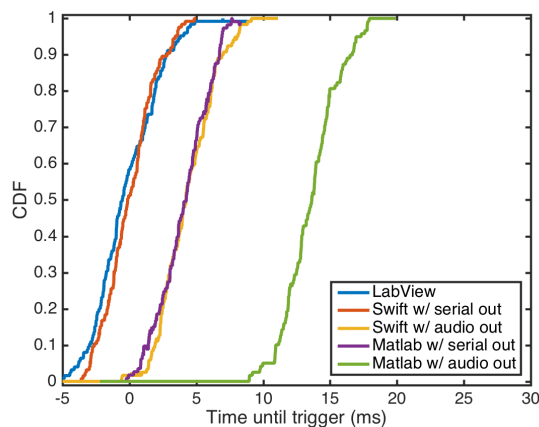


**Figure 7.** Raw timing curves for all detectors measured during detection of  $t_4^*$  using 1.5-ms frames. We extract the trigger events from each curve, from which we obtain the mean—latency—and standard deviation—jitter.

involved in error signaling, given projections from the shelf to AIV, an area known to be critical for processing of sensory errors during singing [19].

The neural-network-based syllable detector enabled this experiment by allowing low-latency AAF triggered off user-selected syllables, without hand-tuning and without relying on harmonic stacks needed for filter-bank-based syllable detection. The detector will allow continued research into the neural encoding of these error signals.

## 4 Discussion

This syllable detector is appropriate for zebra finch song, and although our tests were carried out on songs from that species, it is also likely to work well for Bengalese finches. It offers the following benefits:

- The detector is accurate. False negative and false positive rates can be well under 0.5% and 0.01% respectively, and trading these two numbers off against each other is through a single relative-cost parameter.
- Latency is generally under a millisecond, with jitter around 2 ms.
- Works on a wide range of target syllables using the default values described here, generally eliminating the need for hand-tuning.
- Runs fast enough for syllable-modification experiments on inexpensive

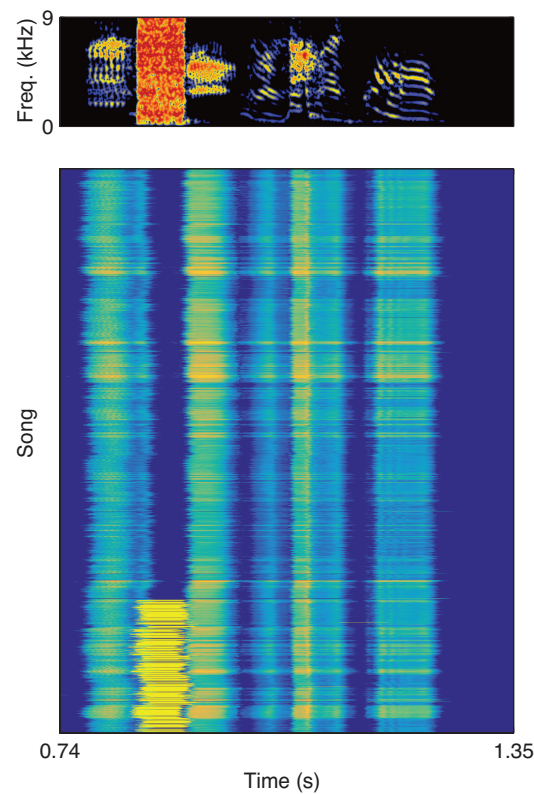


**Figure 8.** Audio amplitude stack plot of the experiment as aligned by the bird's song. The top panel shows a spectrogram of the song with the triggered white-noise stimulus. In the bottom panel, each row is average amplitude for a single performance of the song (1123 songs total). The white-noise stimulus is visible as a bright yellow region after the first syllable in the final quarter of the trials.

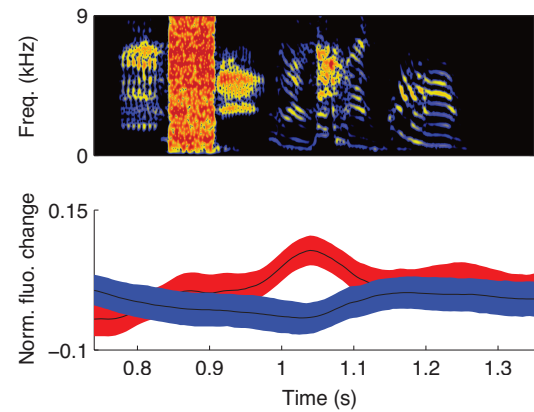


**Figure 9.** Fibre photometry during AAF reveals an AAF-sensitive response (lines indicate mean, shading indicates 95% confidence interval, bootstrap). Blue are catch trials, red are AAF trials.

consumer-grade hardware, although we recommend that the training phase be  
510 run on a fast desktop system with 32 GB of RAM.  
511

- A single detector can generate different target pulses for multiple syllables at  
512 almost no additional computational cost during runtime, although training time  
513 will increase.  
514

Although there are differences, the Swift+serial detector and the LabVIEW  
515 implementation are roughly comparable in performance. We prefer the Swift  
516 implementation due to its lower hardware and software requirements and the difficulty  
517 of debugging LabVIEW programmes. With serial output, MATLAB's performance is  
518 good, although its buffer handling is sensitive to system load.  
519

The song presented here was recorded with a fixed microphone mounted inside the  
520 cage. We found that higher accuracy is achieved when a microphone is instead  
521 mounted on the bird's head, which maintains volume and reduces changes in timbre as  
522 the bird moves.  
523

A common experimental paradigm requires detecting the frequency of syllables.  
524 Many pitch detection techniques rely on the spectrum, which incurs no additional  
525 computational cost here since it is already available. For example, [7] achieved good  
526 results with the Harmonic Product Spectrum algorithm [20].  
527

In order to monitor syllable duration, the beginning and end of a syllable may be  
528 detected by looking at the ratio of total energy in the singing frequency band to the  
529 total energy, over some small time window. Any syllable thus identified that also  
530 contains a trigger event may be monitored for duration. Alternatively, the network  
531 can be trained to recognise both the beginning and the end of the syllable of interest.  
532

In feedback experiments such as frequency- or duration-shifting, vocal output  
533 changes over the course of the experiment. The neural network excels at identifying  
534 syllables close to its training set, so as vocal output changes the detector may not  
535 recognise a match. If the detector must be robust to this shift, it may be retrained as  
536 often as necessary as the bird learns, or data consisting of synthetically pitch-shifted  
537 or duration-shifted target syllables over the recognition region may be added to the  
538 training set. We will test these approaches in future work.  
539

## 5 Acknowledgments

We would like to thank Winthrop F. Gillis, William A. Liberti, and Sanne Moorman for their improvements to the draft. This work was funded by NIH grants 5R01NS089679-02 and 5U01NS090454-02. The funders had no role in study design, data collection and analysis, decision to publish, or preparation of the manuscript.

## A Resources

*If accepted, before final submission, all code will be moved to the Gardner Lab github repository, final release versions generated, and DOIs created as described in https://guides.github.com/activities/citable-code/ so that our results may be reproduced and the software deployed. For now, in lieu of final release DOIs, we provide these links to our development repositories. If you would like final versions and test datasets for review, please contact the corresponding author (bwpearre@bu.edu).*

**Song alignment:** Jeff Markowitz's song alignment software [10] can be found at

<https://github.com/jmarkow/zftftb>

Our implementation of the syllable detector is available under an open-source license (*we are still evaluating which open source license is the most suitable for this software*):

**Training the neural network:**

<https://github.com/bwpearre/birds/align>

**Runtime:**

**MATLAB:** <https://github.com/gardner-lab/syllable-detector-matlab>

**Swift:** <https://github.com/gardner-lab/syllable-detector-swift>

**LabVIEW:** <https://github.com/bwpearre/birds/align>

## References

1. Kao MH, Doupe AJ, Brainard MS. Contributions of an avian basal ganglia–forebrain circuit to real-time modulation of song. Letters to Nature.

- 2005 February;433:638–643. Available from: 565  
<http://www.nature.com/nature/journal/v433/n7026/abs/nature03127.html>. 566
2. Wang CZH, Herbst JA, Keller GB, Hahnloser RHR. Rapid Interhemispheric 567  
Switching during Vo- 568  
cal Production in a Songbird. PLOS Biology. 2008 October;6(10). Available from: 569  
<http://journals.plos.org/plosbiology/article?id=10.1371/journal.pbio.00602>
3. Keller GB, Hahnloser RHR. Neural processing of auditory feedback during 571  
vocal practice in a songbird. Nature. 2009 January;457:187–190. Available from: 572  
<http://www.nature.com/nature/journal/v457/n7226/abs/nature07467.html>. 573
4. Turner EC, Brainard MS. Performance variability enables adaptive plasticity of 574  
'crystallized' adult birdsong. Nature. 2007 December;450:1240–1244. Available 575  
from: 576  
<http://www.nature.com/nature/journal/v450/n7173/abs/nature06390.html>. 577
5. Andalman AS, Fee MS. A basal ganglia-forebrain circuit in the songbird biases 578  
motor output to avoid vocal errors. Proceedings of the National Academy of 579  
Sciences of the United States of America. 2009 July;106(30):12518–12523. 580  
Available from: <http://www.ncbi.nlm.nih.gov/pmc/articles/PMC2709669/>. 581
6. Warren TL, Turner EC, Charlesworth JD, Brainard MS. Mechanisms and time 582  
course of vocal learning and consolidation in the adult songbird. Journal of 583  
Neurophysiology. 2011 October;106(4):1806–1821. Available from: 584  
<http://jn.physiology.org/content/106/4/1806.full>. 585
7. Canopoli A, Herbst JA, Hahnloser RHR. A Higher Sensory Brain Region Is 586  
Involved in Reversing Reinforcement-Induced Vocal Changes in a Songbird. The 587  
Journal of Neuroscience. 2014;34(20):7018–7026. Available from: 588  
<http://www.jneurosci.org/content/34/20/7018.full>. 589
8. Leonardo A, Konishi M. Decrystallization of adult birdsong by perturbation of 590  
auditory feedback. Nature. 1999 June;399:466–470. Available from: 591  
<http://www.nature.com/nature/journal/v399/n6735/abs/399466a0.html>. 592

9. Skocik M, Kozhevnikov A. Real-time system for studies of the effects of acoustic feedback on animal vocalizations. *Frontiers in Neural Circuits*. 2013 January;6(111). Available from: <http://www.ncbi.nlm.nih.gov/pmc/articles/PMC3539774/>. 593  
594  
595  
596
10. Poole B, Markowitz JE, Gardner TJ. The Song Must Go On: Resilience of the Songbird Vocal Motor Pathway. *PLOS One*. 2012 June;7(6). Available from: <http://journals.plos.org/plosone/article?id=10.1371/journal.pone.0038173>. 597  
598
11. Jacobsen E, Lyons R. The sliding DFT. *IEEE Signal Processing Magazine*. 2003 Mar;20(2):74–80. Available from: <http://www.cmlab.csie.ntu.edu.tw/DSPCourse/reference/Sliding%20DFT.pdf> 600  
601  
602
12. Hertz JA, Krogh AS, Palmer RG. *Introduction to the Theory of Neural Computation*. Perseus Books; 1991. 603  
604
13. Markowitz JE, Liberti WA, Guitchounic G, Velho T, Lois C, Gardner TJ. Mesoscopic Patterns of Neural Activity Support Songbird Cortical Sequences. *PLOS Biology*. 2015 June;13(6):e1002158–20. Available from: <http://journals.plos.org/plosbiology/article?id=10.1371/journal.pbio.1002158>. 605  
606  
607
14. Adelsberger H, Garaschuk O, Konnerth A. Cortical calcium waves in resting newborn mice. *Nature Neuroscience*. 2005 August;8(8):988–990. Available from: <http://www.nature.com/neuro/journal/v8/n8/full/nn1502.html>. 609  
610  
611
15. Schulz K, Sydeku E, Krueppel R, Engelbrecht CJ, Schlegel F, Schröter A, et al. Simultaneous BOLD fMRI and fiber-optic calcium recording in rat neocortex. *Nature Methods*. 2012 May;9(6):597–602. Available from: <http://www.nature.com/nmeth/journal/v9/n6/full/nmeth.2013.html>. 612  
613  
614  
615
16. Cui G, Jun SB, Jin X, Pham MD, Vogel SS, Lovinger DM, et al. Concurrent activation of striatal direct and indirect pathways during action initiation. *Nature*. 2013 February;494(7436):238–242. Available from: <http://www.nature.com/nature/journal/v494/n7436/full/nature11846.html>. 616  
617  
618  
619
17. Adelsberger H, Zainos A, Alvarez M, Romo R, Konnerth A. Local domains of motor cortical activity revealed by fiber-optic calcium recordings in behaving 620  
621

- nonhuman primates. Proceedings of the National Academy of Sciences of the United States of America. 2014 January;111(1):463–468. Available from: <http://www.pnas.org/content/111/1/463.full>.
18. Gunaydin LA, Grosenick L, Finkelstein JC, Kauvar IV, Fenno LE, Adhikari A, et al. Natural neural projection dynamics underlying social behavior. Cell. 2014 June;157(7):1535–1551. Available from: <http://www.cell.com/cell/fulltext/S0092-8674%2814%2900659-X>.
19. Mandelblat-Cerf Y, Las L, Denissenko N, Fee M. A role for descending auditory cortical projections in songbird vocal learning. Elife. 2014 January;3(0):e02152–e02152. Available from: <https://elifesciences.org/content/3/e02152>.
20. Noll AM. Pitch determination of human speech by the harmonic product spectrum, the harmonic sum spectrum, and a maximum likelihood estimate. In: Proceedings of the symposium on computer processing in communications. vol. 19; 1970. p. 779–797.